Control Engineering Practice 81 (2018) 244–255

Contents lists available at ScienceDirect

Control Engineering Practice

journal homepage: www.elsevier.com/locate/conengprac

Experimental validation of model predictive control stability for autonomous driving☆

Pedro F. Lima [a,b,*], Gonçalo Collares Pereira [a,b], Jonas Mårtensson [a], Bo Wahlberg [a]

[a] Integrated Transport Research Lab, Department of Automatic Control, School of Electrical Engineering and Computer Science, KTH Royal Institute of Technology, SE-100 44 Stockholm, Sweden

[b] Research and Development, Scania CV AB, 151 87, Södertälje, Sweden

ARTICLE INFO

Keywords:
Model predictive control
Stability
Set invariance
Autonomous driving
Automatic control

ABSTRACT

This paper addresses the design of time-varying model predictive control of an autonomous vehicle in the presence of input rate constraints such that closed-loop stability is guaranteed. Stability is proved via Lyapunov techniques by adding a terminal state constraint and a terminal cost to the controller formulation. The terminal set is the maximum positive invariant set of a multi-plant description of the vehicle linear time-varying model. The terminal cost is an upper-bound on the infinite cost-to-go incurred by applying a linear–quadratic regulator control law. The proposed control design is experimentally tested and successfully stabilizes an autonomous Scania construction truck in an obstacle avoidance scenario.

1. Introduction

Autonomous vehicles will inevitably face emergency situations, in which they may need to maneuver aggressively to avoid, for example, an imminent collision. Road traffic injuries, 94% of which are caused by human error (European Commission, 2011), are predicted to become the third most common cause of disability by 2020 (World Health Organization, 2009). Thus, when removing the human-factor from the equation, ensuring vehicle stability during safety-critical events is of utmost importance when developing commercial autonomous vehicles. Verified stability is a key aspect for safe and reliable autonomous vehicles.

The road to autonomous driving has been slowly paved with the gradual introduction of advanced driving assistant systems (e.g., anti-lock braking system, electronic stability control, adaptive cruise control, lane departure warning system, and automatic parking). These systems play a major role of support to the driver both in critical and tedious situations, reducing the number of traffic accidents and fatalities (Ross, 2014). In particular, ESC intervenes when the steering command given by the driver yields an unstable vehicle motion. Nevertheless, the design of the motion controller module for autonomous vehicles must attain a stable behavior and cannot rely on an eventual unstable behavior being avoided by driving assistance technology. This work addresses the problem of designing motion controllers for autonomous driving that ensure closed-loop stability. In particular, Model Predictive Control (MPC) closed-loop stability issues in practice are investigated. The results show that a standard MPC, without properly designed terminal cost and terminal state set, can lead to instability, particularly when the prediction horizon is short. On the one hand, ensuring vehicle stability facilitates controller certification and standardization when entering the development phase. On the other hand, shortening the prediction horizon gives room to more computational demanding modules. In the first attempts to demonstrate autonomous driving, in the DARPA challenges, the focus was rather in developing a feasible system architecture than in testing the stability limits of the vehicles (Thrun, Montemerlo, Dahlkamp, Stavens, Aron, Diebel, et al., 2006; Urmson, Bagnell, Baker, Hebert, Kelly, Rajkumar, et al., 2007). Even recent vehicle development assume that the vehicle operation is well below handling limits and few or no attention is given to situations of possible vehicle instability (Mchugh, 2015; Ziegler, 0000; Ziegler, Bender, Schreiber, Lategahn, Strauss, Stiller, et al., 2014).

The motion controller is a crucial module in the design of an autonomous vehicle as it is responsible for stabilizing and guiding the vehicle along a given reference path. In the recent decades, MPC has gained increasing attention to address the problem of vehicle control. With the increase of computational power and optimization solvers efficiency, MPC has become quite popular, since it handles nonlinear

☆ This work was supported in part by the Swedish Government and in part by the automotive industry within the FFI program – Strategic Vehicle Research and innovation under Project iQMatic 2012-04626, Vinnova (FFI), Sweden – and by the Wallenberg AI, Autonomous Systems, and Software Program (WASP) funded by Knut and Alice Wallenberg Foundation, Sweden.

* Corresponding author at: Integrated Transport Research Lab, Department of Automatic Control, School of Electrical Engineering and Computer Science, KTH Royal Institute of Technology, SE-100 44 Stockholm, Sweden.

E-mail addresses: pfrdal@kth.se (P.F. Lima), gpcp@kth.se (G. Collares Pereira), jonas1@kth.se (J. Mårtensson), bo@kth.se (B. Wahlberg).

https://doi.org/10.1016/j.conengprac.2018.09.021
Received 1 March 2018; Received in revised form 20 September 2018; Accepted 22 September 2018
Available online 3 October 2018
0967-0661/

time-varying models and constraints in a systematic manner. Using a model to predict the system behavior, an user-defined cost function is minimized, and the optimal sequence of inputs is computed in order to follow a specified path or trajectory under known constraints on states and inputs. A subset of the optimal input sequence is applied to the vehicle and the process is then repeated (Bemporad, 2006; Garcia, Prett, & Morari, 1989; Mayne, Rawlings, Rao, & Scokaert, 2000). One of the strengths of MPC is the possibility of explicitly include additional constraints and cost terms, which lead to closed-loop stability guarantees. One of the most popular strategies for ensuring closed-loop stability using MPC (see Mayne et al., 2000 and references therein) is to use the optimization value function as a Lyapunov function. Moreover, the analysis is convenient if incorporating both a terminal cost and a terminal state set in the optimal control problem. The terminal cost is chosen such that it is equal to the infinite-horizon value function in a suitable neighborhood of the origin (i.e., the terminal state set). Hence, it is possible to use the known advantages of an infinite-horizon control, such as guaranteed stability (Keerthi & Gilbert, 1988).

The closed-loop stability properties when using MPC have been extensively studied from the theoretic point of view (see Mayne et al., 2000 and references therein). However, the lack of implementability of many of the proposed control designs makes the practical analysis less frequent in the literature. When experimental evaluation is considered, the large majority of the works either leave the stability concerns out (Thrun et al., 2006; Urmson et al., 2007), or the vehicle *looks* stable due to careful tuning of controller (Lima, Trincavelli, Mårtensson, Nilsson, and Wahlberg, 2017; Liniger, Domahidi, & Morari, 2015; Turri, Carvalho, Tseng, Johansson, & Borrelli, 2013) or due to the inclusion of vehicle dynamics constraints (Beal & Gerdes, 2013; Falcone, Borrelli, Asgari, Tseng, & Hrovat, 2007; Falcone, Borrelli, Tseng, Asgari, & Hrovat, 2008a; Funke, Brown, Erlien, & Gerdes, 2017; Katriniok, Maschuw, Christen, Eckstein, & Abel, 2013). The scenarios presented range from lane-keeping and obstacle avoidance (Funke et al., 2017; Turri et al., 2013), to racing applications (Beal & Gerdes, 2013; Liniger et al., 2015). Moreover, the presented experiments typically consider low-friction roads (Falcone et al., 2007; Turri et al., 2013) or vehicle handling-limits (Funke et al., 2017; Katriniok et al., 2013). Stability is ensured by constraints that bound the tire slip angle. Consequently, the vehicle motion is bounded within the region of the state space that does not contain unstable vehicle dynamics. Common to all of these schemes is the absence of explicit stability-imposing constraints in the MPC formulations. An exception is (Falcone, Borrelli, Tseng, Asgari, & Hrovat, 2008b), where a stability condition is proposed for a Linear Time-Varying (LTV) MPC scheme used in active front steering systems. An additional convex constraint bounding a quadratic function of the control effort and the predicted states is computed to ensure stability. However, this requires the MPC to be cast as a Sequential Quadratic Program (SQP) that has typically higher computational burden than a QP. Additionally, simplifications are made, such as considering the model time-invariance by linearizing around the current set point and assuming that the terminal state set is a singleton. Although this reduces the complexity of the overall design, it also affects the feasibility region of the controller.

1.1. Main contributions

The main contributions of this paper are:

1. the offline computation of the terminal cost and terminal state set for linear time-varying model predictive controller (LTV-MPC) closed-loop stability;
2. the proof of LTV-MPC closed-loop stability using the novel terminal cost and terminal state set;
3. the interpretation of the MPC parameter tuning influence in the design of the terminal cost and terminal state set in the autonomous driving case;
4. the effectiveness of the proposed control design in an autonomous Scania construction truck in simulation and experimentally.

The work presented here is an extension of Lima, Mårtensson, and Wahlberg (2017), where closed-loop stability is proved when using and LTV-MPC to lateral control an autonomous truck. There, a nonlinear kinematic vehicle model is linearized around a reference path, yielding an LTV model. The vehicle is modeled in the spatial domain and in a road-aligned coordinate frame with respect to a reference path to exclude time and speed from the dynamics equations (Frasch, Gray, Zanon, Ferreau, Sager, Borrelli, et al., 2013; Gao, Gray, Frasch, Lin, Tseng, Hedrick, et al., 2012; Lima, Oliveira, Mårtensson, Bemporad, and Wahlberg, 2017; Plessen, Lima, Mårtensson, Bemporad, & Wahlberg, 2017; Verschueren, De Bruyne, Zanon, Frasch, & Diehl, 2014). That work used the notion of multi-plant description (Badgwell & Thomas, 1997; Kothare, Balakrishnan, & Morari, 1996), in which the LTV model is divided in several Linear Time-Invariant (LTI) models. Moreover, it proposes that the maximum positive invariant set of over all the LTI models in the multi-plant description would be the terminal state set. The terminal cost was computed solving a convex min–max optimization problem (Lu & Arkun, 2000) that leads to the determination of the *worst* time-invariant model if used as a prediction model.

In this work, the notions of multi-plant description and space-based road-aligned vehicle model are used again. In addition to Lima and Mårtensson et al. (2017), this work

1. presents a new approach for computing the terminal cost;
2. proposes terminal cost and terminal state set considering input rate constraints;
3. shows the experimental evaluation of the proposed control design.

In this paper, the terminal cost is proposed to be the upper-bound on the cost-to-go incurred by applying a Linear–Quadratic Regulator (LQR) control law to any of the possible models in the multi-model representation. An upper-bound can be obtained by positively scaling one of Riccati matrices resulting from the cost-to-go calculation, which considers that the vehicle model is contained inside a convex uncertainty polytope. Moreover, including input rate constraints adds one extra dimension to both the terminal state set and weight matrix. This extra dimension is the input and it plays a major role in ensuring vehicle stability. With the proposed cost and state set design, stability and feasibility of the proposed LTV-MPC scheme are theoretically proved. The MPC parameter tuning influence is discussed in the light of autonomous driving. The effectiveness of the proposed MPC design is evaluated in simulation and in real experiments with a construction Scania truck in a scenario that resembles an emergency maneuver, where the vehicle avoids a fictitious obstacle. The controller successfully stabilizes an autonomous Scania construction truck even when other controllers, with no or milder terminal cost and terminal state set, cannot do it.

The development of the methods presented in this paper has in mind their practical applicability. Therefore, including the terminal cost and terminal state set in the control design should neither affect the execution time nor the optimization convexity. However, offline-computed solutions may be conservative as they need to cover a larger set of scenarios *a priori*, rather than computing less conservative terminal cost and terminal state set online.

1.2. Outline

The remainder of this paper is organized as follows. Section 2 introduces theoretical preliminaries; Section 3 addresses the problem of reference tracking using a receding-horizon framework by developing an LTV-MPC controller; Section 4 presents the nonlinear space-based vehicle model in the road-aligned coordinate frame used in the autonomous driving example. Furthermore, the same section proposes the terminal cost and terminal state set, which are used for proving

LTV-MPC feasibility and closed-loop stability in Section 5; Section 6 demonstrates the effectiveness of the inclusion of the terminal cost and terminal state set in the MPC design through simulations and experiments. Section 7 provides some concluding remarks and outlines future work.

2. Preliminaries

This section introduces the main concepts that are used throughout the paper. It follows the structure and notation of Borrelli, Bemporad, and Morari (2017).

This paper deals with discrete-time nonlinear systems subject to external inputs:

$$\mathbf{z}(k+1) = f\big(\mathbf{z}(k), \mathbf{u}(k)\big), \tag{1}$$

where $\mathbf{z}(k) \in \mathbb{R}^n$ and $\mathbf{u}(k) \in \mathbb{R}^m$ are the state and input vectors, respectively. Both systems are subject to state and input constraints

$$\mathbf{z}(k) \in \mathcal{Z}, \mathbf{u}(k) \in \mathcal{U}, \forall k \in \mathbb{N}_+, \tag{2}$$

where the sets $\mathcal{Z} \subseteq \mathbb{R}^n$ and $\mathcal{U} \subseteq \mathbb{R}^m$ are polytopes.

When system (1) is subject to the feedback control law $\mathbf{u}(k) = \mathbf{l}(k)\mathbf{z}(k)$, where $\mathbf{l}(k)$ is a time-varying feedback control gain, the discrete-time autonomous system becomes

$$\mathbf{z}(k+1) = f_a\big(\mathbf{z}(k)\big) = f\big(\mathbf{z}(k), \mathbf{l}(k)\big). \tag{3}$$

Definition 1 (*One-step Controllable Set*)**.** For system (1), the one-step controllable set to the set S is denoted as

$$\mathrm{Pre}(S) = \{z \in \mathbb{R}^n : \exists u \in \mathcal{U}, f(\mathbf{z}, \mathbf{u}) \in S\}. \tag{4}$$

$\mathrm{Pre}(S)$ is the set of states that evolve into the target set S in one time step.

Definition 2 (N-*step Controllable Set*)**.** For a given target set $S \subseteq \mathcal{Z}$, the N-step controllable set $\mathcal{K}_N(S)$ of system (1) subject to the constraints (2) is defined recursively as

$$\mathcal{K}_j(S) = \mathrm{Pre}\big(\mathcal{K}_{j-1}(S)\big) \cap \mathcal{Z},\ \mathcal{K}_0(S) = S,\ j = \{1, \dots, N\}. \tag{5}$$

All states of system (3) belonging to the N-step controllable set $\mathcal{K}_N(S)$ evolve to the target set S in N steps, while satisfying the constraints.

Definition 3 (*Positive Invariant Set*)**.** A set $\mathcal{O} \subseteq \mathcal{Z}$ is said to be a positive invariant set for system (3) subject to the constraints in (2), if

$$\mathbf{z}(0) \in \mathcal{O} \Rightarrow \mathbf{z}(k) \in \mathcal{O}, \forall k \in \mathbb{N}_+.$$

For a given feedback controller $u(k) = \mathbf{l}(k)\mathbf{z}(k)$, $\mathcal{O}$ is the set of initial states whose trajectory will never violate the system constraints.

Definition 4 (*Maximal Positive Invariant Set*)**.** The set $\mathcal{O}^\infty \subseteq \mathcal{Z}$ is the maximal positive invariant set of the autonomous system (3) subject to the constraints in (2) if $\mathcal{O}^\infty$ is invariant and contains all the invariant sets contained in $\mathcal{Z}$.

Theorem 2.1 (*Geometric Condition for Invariance*)**.** *A set $\mathcal{O} \subseteq \mathcal{Z}$ is a positive invariant set for the autonomous system (3) subject to the constraints in (2) if and only if*

$$\mathcal{O} \subseteq \mathrm{Pre}(\mathcal{O}), \tag{6}$$

A proof is found in Borrelli et al. (2017).

In other words, if the system (3) is inside $\mathcal{O}$, it will remain there while respecting the constraints (2).

3. Linear time-varying model predictive control

Consider the problem of controlling the discrete-time nonlinear time-varying system (1) with constraints (2) to track a given time-varying reference. Consider the reference state $\mathbf{z}_r(k) \in \mathcal{Z}$ and the input $\mathbf{u}_r(k) \in \mathcal{U}$. Let $\bar{Z}_r(k) = \{\mathbf{z}_r(k), \mathbf{z}_r(k+1), \dots\}$ be the reference state path obtained by applying an input sequence $\bar{U}_r(k) = \{\mathbf{u}_r(k), \mathbf{u}_r(k+1), \dots\}$ for $k \geq 0$ to system (1). Then, the first-order Taylor approximation and forward Euler discretization of (1) around $\bar{Z}_r(k)$ and $\bar{U}_r(k)$ yields a linear time-varying (or linear space-varying) system that can be written in the following form

$$\tilde{\mathbf{z}}(k+1) = \mathbf{A}\big(\boldsymbol{\xi}(k)\big)\tilde{\mathbf{z}}(k) + \mathbf{B}\big(\boldsymbol{\xi}(k)\big)\tilde{\mathbf{u}}(k), \tag{7}$$

where $\tilde{\mathbf{z}}(k) = \mathbf{z}(k) - \mathbf{z}_r(k)$ and $\tilde{\mathbf{u}}(k) = \mathbf{u}(k) - \mathbf{u}_r(k)$ and

$$\mathbf{A}\big(\boldsymbol{\xi}(k)\big) = \left.\frac{\partial f(\mathbf{z}, \mathbf{u})}{\partial \mathbf{z}}\right|_{\substack{\mathbf{z} = \mathbf{z}_r(k), \\ \mathbf{u} = \mathbf{u}_r(k)}}, \mathbf{B}\big(\boldsymbol{\xi}(k)\big) = \left.\frac{\partial f(\mathbf{z}, \mathbf{u})}{\partial \mathbf{u}}\right|_{\substack{\mathbf{z} = \mathbf{z}_r(k), \\ \mathbf{u} = \mathbf{u}_r(k)}}, \tag{8}$$

where $\boldsymbol{\xi}(k)$ is a parameter vector of the form $\boldsymbol{\xi}(k) = [\mathbf{z}_r(k), \mathbf{u}_r(k)]^T$, which is known at every step k. Also, $\boldsymbol{\xi}(k) \in \Xi$ for each k, where Ξ is a closed set containing all the possible values of $\boldsymbol{\xi}$ such that

$$\Xi = \{\boldsymbol{\xi} \in \mathbb{R}^{n+m} : \boldsymbol{\xi}_{\min} \leq \boldsymbol{\xi} \leq \boldsymbol{\xi}_{\max}\}, \tag{9}$$

where the inequality operations are considered element-wise. The LTV system (7) is a first-order approximation of the nonlinear system (1). It describes the deviations from the reference path $\bar{Z}_r(k)$ when a sequence of inputs $\bar{U}_r(k)$ is applied to the system.

Let $\gamma \in \Gamma$ represent a model described by a specific pair $(\mathbf{A}(\boldsymbol{\xi}), \mathbf{B}(\boldsymbol{\xi}))$, where the set Γ is a multi-plant description defined as

$$\Gamma = \{(\mathbf{A}, \mathbf{B}) \in \mathbb{R}^{n \times n} \times \mathbb{R}^{n \times m} : \mathbf{A} = \mathbf{A}(\boldsymbol{\xi}), \mathbf{B} = \mathbf{B}(\boldsymbol{\xi}), \boldsymbol{\xi} \in \Xi\}. \tag{10}$$

Note that each $\gamma \in \Gamma$ is time-invariant and depends on a (known) parameter $\boldsymbol{\xi}$.

Assume that a full measurement or estimate of the state $\mathbf{z}(t)$ is available at the current time t. Then, the following MPC problem can be formulated

$$\min_{\tilde{U}_t} \quad \tilde{\mathbf{z}}_{t+N|t}^T \mathbf{Q}_f \tilde{\mathbf{z}}_{t+N|t} + \sum_{k=t}^{t+N-1} \tilde{\mathbf{z}}_{k|t}^T \mathbf{Q} \tilde{\mathbf{z}}_{k|t} + \tilde{\mathbf{u}}_{k|t}^T \mathbf{R} \tilde{\mathbf{u}}_{k|t} \tag{11a}$$

$$\text{subject to} \quad \tilde{\mathbf{z}}_{k+1|t} = \mathbf{A}\big(\boldsymbol{\xi}(k|t)\big)\tilde{\mathbf{z}}_{k|t} + \mathbf{B}\big(\boldsymbol{\xi}(k|t)\big)\tilde{\mathbf{u}}_{k|t},\ k = t, \dots, t+N-1, \tag{11b}$$

$$\tilde{\mathbf{z}}_{k|t} \in \tilde{\mathcal{Z}},\ k = t, \dots, t+N-1, \tag{11c}$$

$$\mathbf{u}_{k|t} \in \mathcal{U},\ k = t, \dots, t+N-1, \tag{11d}$$

$$\tilde{\mathbf{z}}_{t+N|t} \in \tilde{\mathcal{Z}}_f, \tag{11e}$$

$$\tilde{\mathbf{z}}_{t|t} = \tilde{\mathbf{z}}(t), \tag{11f}$$

where $\tilde{U}_t = \{\tilde{\mathbf{u}}_{t|t}, \dots, \tilde{\mathbf{u}}_{t+N-1|t}\}$ is the sequence of inputs to be optimized, which are constrained to be in a convex polytope $\mathcal{U}$. The difference between the state vector at time $t+k$ predicted at time t and the reference state vector $\mathbf{z}_r(t+k)$ is defined by $\tilde{\mathbf{z}}_{t+k|t}$. The difference between the predicted and the reference state is constrained to be in a convex polytope $\tilde{\mathcal{Z}}$. Here, the notation $\mathbf{z}_{t+k|t}$ stands for "the state $\mathbf{z}$ at time $t+k$ predicted at time t". The notation is analogous for $\mathbf{u}_{t+k|t}$. Note that $\mathbf{z}(t)$ is then the actual state $\mathbf{z}$ at time t. The matrices $\mathbf{R}$, $\mathbf{Q}$, and $\mathbf{Q}_f$ are positive definite and penalize deviations from the reference input, state, and terminal state, respectively.

Remark. It is assumed that a full measurement or estimate of the state $\mathbf{z}(t)$ is available at the current time t. However, this is not always the case for the real application, since time delays are almost unavoidable in the real system. In fact, the construction vehicle, in which the controller is deployed, presents a time delay (Lima and Trincavelli et al., 2017). In our controller design, the delay present in the system is not explicitly

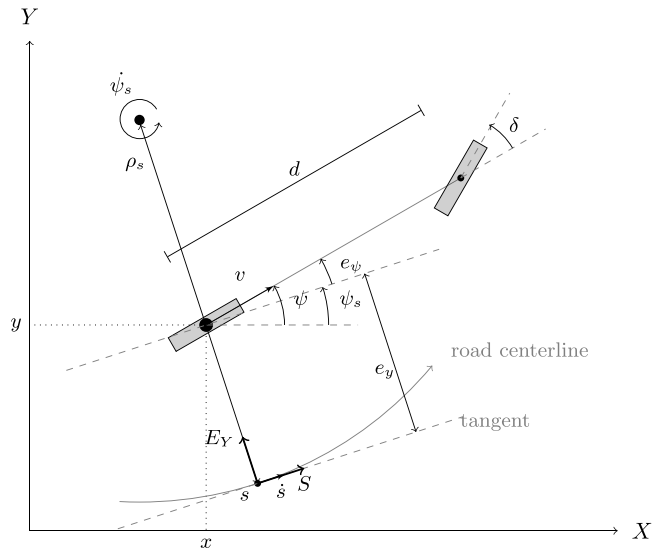

Fig. 1. A nonlinear dynamic bicycle model including the representation of the road-aligned coordinate system.

accounted for. Nevertheless, to deal with it, the vehicle state after the time delay is estimated and used as the current state $\mathbf{z}(t)$. Future work includes MPC design that explicitly accounts for possible delays present in the system (Ai, Sentis, Paine, Han, Mok, & Fok, 2016).

Let $\tilde{U}_t^\star = \{\tilde{\mathbf{u}}_{t|t}^\star, \dots, \tilde{\mathbf{u}}_{t+N-1|t}^\star\}$ be the optimal solution of (11) at time t. The first element of $\tilde{U}_t^\star$ is applied to system (7) at time t. In the next sampling time, the optimal control problem (11) is solved again using the new state measurements, and the horizon is shifted forward. This is also called receding-horizon control.

In receding-horizon control, the optimization problem may lead us into an infeasible situation (i.e., there does not exist a sequence of control inputs for which the constraints are satisfied). Also, even if the optimization problem is always feasible, the computed optimal control inputs may not lead to an asymptotically stable closed-loop system. In general, feasibility and closed-loop stability are not ensured in (11).

This work studies how the terminal weight $\mathbf{Q}_f$ and the terminal constraint set $\tilde{\mathcal{Z}}_f$ should be chosen such that closed-loop stability and feasibility are ensured for all $\gamma \in \Gamma$. Conditions on how the terminal weight $\mathbf{Q}_f$ and the terminal constraint set $\tilde{\mathcal{Z}}_f$ should be chosen such that closed-loop stability and feasibility are ensured have been extensively studied in the past three decades (Mayne et al., 2000). The main idea is to find a feedback control law $\mathbf{l}(k)$ that stabilizes the unconstrained system (7) inside an invariant terminal region $\tilde{\mathcal{Z}}_f$. Then, the closed-loop is stable if the cost function (11a) accounts for the infinite-horizon cost. The finite-horizon cost (when the controller is constrained) is added to the infinite-horizon cost (when the controller is unconstrained (i.e., when the system enters $\tilde{\mathcal{Z}}_f$)). Then, for an unconstrained linear system the convergence to the origin is exponential (Borrelli et al., 2017).

4. MPC design for autonomous driving

This section particularizes the general framework presented in Section 3 to an autonomous driving application.

4.1. Space-based vehicle model

Fig. 1 depicts the relation between the global and the road-aligned coordinate frames. The derivation of the space-based vehicle model follows Gao et al. (2012). The main idea is to introduce the variable s representing the distance along the reference and model the lateral e_y and heading displacement e_ψ between the vehicle and the road as a function of the space s.

Let us start by defining the vehicle model in the time-domain. The movement of a car-like nonholonomic vehicle at low speeds (i.e., when the lateral dynamics have negligible influence) is approximately described by its time-domain kinematic equations (De Luca, Oriolo, & Samson, 1998) given by

$$\begin{aligned} \dot{x} &= \frac{\mathrm{d}x}{\mathrm{d}t} = v\cos(\psi), \\ \dot{y} &= \frac{\mathrm{d}y}{\mathrm{d}t} = v\sin(\psi), \\ \dot{\psi} &= \frac{\mathrm{d}\psi}{\mathrm{d}t} = \frac{v}{d}\tan(\delta), \end{aligned} \tag{12}$$

where x and y are the coordinates of the vehicle in the global coordinate system, ψ is the yaw angle, d is the distance between the front and rear axle, v is the longitudinal velocity in the vehicle coordinate system, and δ is the steering angle of the front wheels. The vehicle curvature κ is related with the vehicle steering angle δ by $\kappa = \frac{\tan(\delta)}{d}$.

Accordingly to Fig. 1, the geometric relations are

$$\begin{aligned} \dot{e}_y &= v\sin(e_\psi), \\ \dot{e}_\psi &= \dot{\psi} - \dot{\psi}_s, \\ \dot{s} &= \frac{\rho_s v\cos(e_\psi)}{\rho_s - e_y}, \end{aligned} \tag{13}$$

where ρ_s is the radius of curvature of the road and ψ_s is the road heading angle.

Assuming that $v \neq 0$ and that it is a continuous function, and observing that the spatial derivative can be expressed as a function of the time derivative, namely $\frac{\mathrm{d}(\cdot)}{\mathrm{d}s} = \frac{\mathrm{d}(\cdot)}{\mathrm{d}t}\frac{\mathrm{d}t}{\mathrm{d}s} = \frac{\mathrm{d}(\cdot)}{\mathrm{d}t}\frac{1}{\dot{s}}$, the space-based representation of (12) can then be derived as

$$\begin{aligned} e_y' &= \frac{\dot{e}_y}{\dot{s}} = \frac{\rho_s - e_y}{\rho_s}\tan(e_\psi), \\ e_\psi' &= \frac{\dot{e}_\psi}{\dot{s}} = \frac{(\rho_s - e_y)}{\rho_s\cos(e_\psi)}\kappa - \psi_s'. \end{aligned} \tag{14}$$

The nonlinear model (14) is linearized and discretized (with $\Delta s = vT_s$, where T_s is the sampling period, and v is the current vehicle speed and is constant throughout the prediction horizon) around a reference path $\mathbf{z}_r(k) = [e_{y,r}(k), e_{\psi,r}(k)]^T = [0,0]^T$ for all $k \geq 0$ given by a reference sequence of inputs $\bar{U}_r(k)$. Thus, obtaining a LTV model of the form (7)

$$\begin{bmatrix} e_y(k+1) \\ e_\psi(k+1) \end{bmatrix} = \begin{bmatrix} 1 & \Delta_s \\ -\kappa_r^2(k)\Delta_s & 1 \end{bmatrix}\begin{bmatrix} e_y(k) \\ e_\psi(k) \end{bmatrix} + \begin{bmatrix} 0 \\ \Delta_s \end{bmatrix}\tilde{\kappa}(k), \tag{15}$$

where it is assumed that the reference input curvature $\kappa_r = \kappa_s = \frac{1}{\rho_s}$. The parameter $\boldsymbol{\xi}(k)$ is, in this particular case, only dependent on the road curvature $\kappa_r(k)$. In fact, Δ_s could also be seen as a parameter, but in the analysis it is set as constant (i.e., the vehicle travels with constant speed). Consequently, in the remainder of the paper and for the sake of notation simplicity, $\boldsymbol{\xi}(k) = \kappa_r(k)$.

In summary, the MPC formulation (11) is used to control a nonholonomic vehicle to the given reference using a linearized and discretized space-based kinematic vehicle model (15). The state vector is $\tilde{\mathbf{z}}(k) = [e_y(k), e_\psi(k)]^T$ and the input is $\tilde{\mathbf{u}}(k) = \tilde{\kappa}(k) = \kappa(k) - \kappa_r(k)$. Therefore, knowing the reference curvature $\kappa_s(k)$ *a priori* allows the definition of the set $\boldsymbol{\xi}$, where $\boldsymbol{\xi}_{\min} = \kappa_{r,\min}$ and $\boldsymbol{\xi}_{\max} = \kappa_{r,\max}$. Constraining the terminal state of the MPC prediction horizon to lie inside the terminal constraint set $\tilde{\mathcal{Z}}_f$ and properly choosing $\mathbf{Q}_f$, closed-loop stability and feasibility are ensured for all $\gamma \in \Gamma$.

4.2. Computation of the terminal constraint $\tilde{\mathcal{Z}}_f$

When the model is LTI, a typical choice for $\tilde{\mathcal{Z}}_f$ is the maximal positive invariant set $\mathcal{O}_\infty^{\mathrm{LQR}}$ for the closed-loop system

$$\tilde{\mathbf{z}}(k+1) = \Big(\mathbf{A}\big(\boldsymbol{\xi}(k)\big) + \mathbf{B}\big(\boldsymbol{\xi}(k)\big)\mathbf{l}_{\mathrm{LQR}}\big(\boldsymbol{\xi}(k)\big)\Big)\tilde{\mathbf{z}}(k), \tag{16}$$

where $\mathbf{l}_{\mathrm{LQR}}$ is the associated LQR gain (i.e., the unconstrained infinite time optimal controller gain).

However, since our model is LTV, there are several maximal positive invariant sets $\mathcal{O}_{\infty}^{\mathrm{LQR}}(\gamma)$ and several different LQR feedback controllers $\mathbf{l}_{\mathrm{LQR}}(\xi)$, one for each $\xi \in \Xi$. Therefore, the maximal positive invariant set $\bar{\mathcal{O}}_{\infty}^{\mathrm{LQR}}$ that is invariant for all $\gamma \in \Gamma$ is sought (i.e., $\bar{\mathcal{O}}_{\infty}^{\mathrm{LQR}} \subseteq \mathrm{Pre}_{\gamma}(\bar{\mathcal{O}}_{\infty}^{\mathrm{LQR}})$, $\forall \gamma \in \Gamma$). The notation $\mathrm{Pre}_{\gamma}(\cdot)$ denotes the one-step controllable set (see Definition 1) using a specific model γ.

Recall the geometric condition for invariance expressed in Theorem 2.1 and let Γ_d be a discretized version of the multi-plant Γ with a finite number of LTI models. Then, the following recursion

$$\Omega_{k+1} = \bigcap_{\gamma \in \Gamma_d} \mathrm{Pre}_{\gamma}(\Omega_k) \cap \Omega_k, \ \Omega_0 = \tilde{\mathcal{Z}}, \tag{17}$$

eventually converges to the maximal positive invariant set (see Definition 4) (Kolmanovsky & Gilbert, 1998), i.e.,

$$\bar{\mathcal{O}}_{\infty}^{\mathrm{LQR}} = \lim_{k \to \infty} \Omega_k. \tag{18}$$

Note that, the matrix $\mathbf{A}\big(\xi(k)\big)$ of model (15) can be described as belonging to a convex uncertainty polytope

$$\Lambda = \{\mathbf{A} \in \mathbb{R}^{2\times 2} : \mathbf{A} = \sum_{i=1}^{2} \lambda_i \mathbf{A}_i, \sum_{i=1}^{2} \lambda_i = 1, \lambda_i \geq 0\}. \tag{19}$$

Therefore, it is possible to show that a polyhedral robust invariant set (i.e., robust with respect to the varying parameter) can be constructed only using the vertices of the uncertainty polytope (Blanchini, 1999; Pluymers, Rossiter, Suykens, & De Moor, 2005). In other words, if Γ_d includes, at least, the vertices of $\mathbf{A}\big(\xi(k)\big)$, then (17) computes the maximum invariant set of Γ.

All the operations with sets are performed using the Multi-Parametric Toolbox (MPT) for MATLAB (Kvasnica, Grieder, Baotić, & Morari, 2004).

Computation of $\bar{\mathcal{O}}_{\infty}^{\mathrm{LQR}}$ without input rate constraints

Fig. 2 (left plot) depicts an example of the computation of a $\bar{\mathcal{O}}_{\infty}^{\mathrm{LQR}}$ for model (15), where the input is saturated outside −0.18 and 0.18 m^{-1}, which are the curvature limits of the construction truck later considered in the experimental evaluation. The vehicle and tuning parameters used are $|\kappa_r| \leq 0.18\ \mathrm{m}^{-1}$, $\mathbf{Q} = I$, $\mathbf{R} = 1$, and $\Delta s = 1$ m. The figure also shows some $\mathcal{O}_{\infty}^{\mathrm{LQR}}$ for different κ_r. The geometric interpretation of the computed set is intuitive. If the vehicle is on the *left* of the path (positive e_y), the heading displacement e_ψ tends to be negative, so that the vehicle tends to point *inwards* to the path, and vice-versa. For the model (15), in average, each LTI invariant sets take around 0.2 s to compute and the LTV invariant set takes around 1 s.

Since $\bar{\mathcal{O}}_{\infty}^{\mathrm{LQR}}$ is a convex polytope set, the constraint (11e) can be written as

$$\mathbf{H}\tilde{\mathbf{z}}_{t+N|t} \leq \mathbf{h}, \tag{20}$$

where $\mathbf{H} \in \mathbb{R}^{2\times h_n}$ and $\mathbf{h} \in \mathbb{R}^{h_n}$, where h_n represents the number of planes that define the set.

Computation of $\bar{\mathcal{O}}_{\infty}^{\mathrm{LQR}}$ with input rate constraints

When the input rate constraints are considered, the LTI invariant sets $\mathcal{O}_{\infty}^{\mathrm{LQR}}$ and the LTV invariant sets $\bar{\mathcal{O}}_{\infty}^{\mathrm{LQR}}$ also depend on the input curvature κ (see right plot in Fig. 2). The input rate is saturated outside 0.05 and 0.05 m^{-1}/s, and the vehicle and tuning parameters used are the same as before. Again, if the vehicle is on the *left* of the path (positive e_y), the heading displacement e_ψ tends to be negative, and the curvature κ tends to be positive, so that the vehicle always curves *towards* the path, and vice-versa. For model (15), in average, each LTI invariant sets take around 0.3 s to compute and the LTV invariant set takes 1.5 s. So, it seems that the computational time of the invariant sets is linearly proportional to the number of states used.

In this case, $\bar{\mathcal{O}}_{\infty}^{\mathrm{LQR}}$ is also a convex set, but with one extra dimension. So the constraint (11e) can be written as

$$\mathbf{H}\tilde{\mathbf{z}}_{t+N|t} + \mathbf{G}\tilde{\mathbf{u}}_{t+N-1|t} \leq \mathbf{h}, \tag{21}$$

where $\mathbf{H} \in \mathbb{R}^{2\times h_n}$, $\mathbf{G} \in \mathbb{R}^{1\times h_n}$ and $\mathbf{h} \in \mathbb{R}^{h_n}$, where h_n represents the number of hyperplanes that define the set.

Influence of the penalization matrices $\mathbf{Q}$ *and* $\mathbf{R}$

This section discusses the influence of the penalization matrices $\mathbf{Q}$ and $\mathbf{R}$ in the computation of $\bar{\mathcal{O}}_{\infty}^{\mathrm{LQR}}$, with and without input rate constraints.

Fig. 3 shows the influence of $\mathbf{R}$ and $\mathbf{Q}$ on the shape of $\bar{\mathcal{O}}_{\infty}^{\mathrm{LQR}}$. The larger the deviations from the reference input (reflected in $\mathbf{R}$) are penalized, the larger the LTV invariant set $\bar{\mathcal{O}}_{\infty}^{\mathrm{LQR}}$. A large terminal set is desired, since the feasibility region, in which stability can be ensured, is larger. In any case, it is not necessary to ensure stability in cases where the vehicle is too far away from the reference. The higher the cost of being far from the reference (i.e., increasing Q_{11}, the first diagonal element of $\mathbf{Q}$), the smaller the invariant set. This is expected, since if the lateral deviation from the reference is highly penalized, the controller becomes too aggressive, resulting in a smaller invariant set and, consequently, in a smaller attraction region, which can cause infeasibility problems. Finally, the influence of the heading displacement penalization (i.e., Q_{22}, the second diagonal element of $\mathbf{Q}$) is reflected in a larger e_y region covered and smaller e_ψ region covered. The interpretation lies in the fact that, if heading displacement is expensive, then the invariant set avoids including large e_ψ. The tuning of the state penalization matrix $\mathbf{Q}$ does not influence significantly the LTV invariant set curvature range, while in the case of the input penalization matrix $\mathbf{R}$ it clearly does.

Influence of speed

Assuming constant speed within the prediction horizon distance is a valid assumption, since in autonomous heavy duty-vehicle applications the driving should not be aggressive and the vehicle has (very) slow dynamics. However, the vehicle drives at different speeds, so it is relevant to investigate how different velocities influence the shape of the maximum positive invariant set of the system (15) with and without input rate constraints. The maximum positive invariant set for a discretized set of speeds can be computed offline and stored in a look-up table. Then, depending on the current vehicle speed, the terminal state constraint is chosen accordingly online. Fig. 4 shows different $\bar{\mathcal{O}}_{\infty}^{\mathrm{LQR}}$ for different speeds (equivalently the sampling distance Δ_s, since the sampling time is maintained constant $T_s = 0.1$ s). It can be seen that the higher the speed the more skewed the shape of the invariant set. As the speed increases, the prediction distance also increases and consequently, the invariant set is typically larger allowing larger e_ψ that are directly correlated with larger e_y. Note that, when input rate constraints are considered, the set curvature range is significantly reduced for higher speeds. This is logical and a desired behavior as the vehicle travels faster (i.e., takes less time to travel the same distance) and, therefore, is able to steer less within the same distance.

4.3. Computation of the terminal cost $\mathbf{Q}_f$

When the model is LTI (i.e., for a specific $\xi \in \Xi$), it can be shown that the control law $\mathbf{u}(t) = \mathbf{l}_{\mathrm{LQR}}\big(\xi(t)\big)\tilde{\mathbf{z}}(t)$ results in an infinite-horizon cost given by

$$J_{\infty}^{*}\big(\tilde{\mathbf{z}}(t)\big) = \tilde{\mathbf{z}}(t)^T \mathbf{P}\big(\xi(t)\big)\tilde{\mathbf{z}}(t) = \sum_{k=t}^{\infty} \tilde{\mathbf{z}}_{k|t}^T \mathbf{Q}\tilde{\mathbf{z}}_{k|t} + \tilde{\mathbf{u}}_{k|t}^T \mathbf{R}\tilde{\mathbf{u}}_{k|t}, \tag{22}$$

where $\mathbf{P}(\xi)$ is given by the solution of the algebraic Riccati equation for the system (7) for a specific $\xi \in \Xi$, i.e.,

$$\mathbf{A}(\xi)^T \Big(\mathbf{P}(\xi) - \mathbf{P}(\xi)\mathbf{B}(\xi)\big(\mathbf{B}(\xi)^T \mathbf{P}(\xi)\mathbf{B}(\xi) + \mathbf{R}\big)^{-1}\mathbf{B}(\xi)\mathbf{P}(\xi)\Big)\mathbf{A}(\xi) + \mathbf{Q} - \mathbf{P}(\xi) = 0, \tag{23}$$

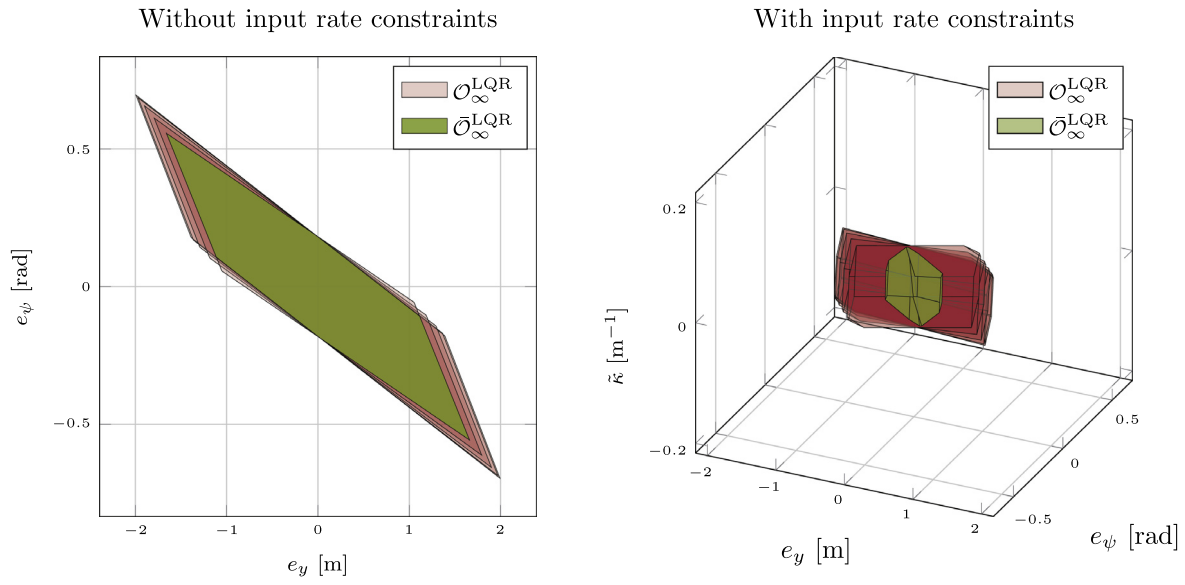

Fig. 2. Maximal positive invariant set for each (red) LTI vehicle model and for all (green) LTI vehicle models.

which can be rewritten as

$$\mathbf{A}_{\mathrm{cl}}(\xi)^T\mathbf{P}(\xi)\mathbf{A}_{\mathrm{cl}}(\xi)+\mathbf{l}_{\mathrm{LQR}}(\xi)^T\mathbf{R}\mathbf{l}_{\mathrm{LQR}}(\xi)+\mathbf{Q}-\mathbf{P}(\xi)=0, \tag{24}$$

where $\mathbf{A}_{\mathrm{cl}}(\xi) = \big(\mathbf{A}(\xi)+\mathbf{B}(\xi)\mathbf{l}_{\mathrm{LQR}}(\xi)\big)$. Therefore, the terminal cost $\tilde{\mathbf{z}}_{t+N|t}^T\mathbf{Q}_f\tilde{\mathbf{z}}_{t+N|t}$ is typically chosen as the solution of the algebraic Riccati equation for the system (7) for a given $\xi\in\Xi$.

The determination of an upper-bound of the infinite-horizon predicted cost for all $\gamma\in\Gamma$ is fundamental to prove LTV-MPC closed-loop stability through Lyapunov techniques. In other words, a $\bar{\mathbf{P}}$ such that

$$\mathbf{A}_{\mathrm{cl}}(\xi)^T\bar{\mathbf{P}}\mathbf{A}_{\mathrm{cl}}(\xi)+\mathbf{l}_{\mathrm{LQR}}(\xi)^T\mathbf{R}\mathbf{l}_{\mathrm{LQR}}(\xi)+\mathbf{Q}-\bar{\mathbf{P}}\preceq 0,\ \forall\xi\in\Xi, \tag{25}$$

is sought. Note that, from (24)

$$\mathbf{l}_{\mathrm{LQR}}(\xi)^T\mathbf{R}\mathbf{l}_{\mathrm{LQR}}(\xi)+\mathbf{Q}=\mathbf{P}(\xi)-\mathbf{A}_{\mathrm{cl}}(\xi)^T\mathbf{P}(\xi)\mathbf{A}_{\mathrm{cl}}(\xi), \tag{26}$$

then (25) can be rewritten as

$$\mathbf{A}_{\mathrm{cl}}(\xi)^T\big(\bar{\mathbf{P}}-\mathbf{P}(\xi)\big)\mathbf{A}_{\mathrm{cl}}(\xi)-\big(\bar{\mathbf{P}}-\mathbf{P}(\xi)\big)\preceq 0,\ \forall\xi\in\Xi. \tag{27}$$

Our previous work (Lima and Mårtensson et al., 2017) proposes $\bar{\mathbf{P}}$ should be chosen as $\bar{\mathbf{P}}=\mathbf{P}(\xi^\star)$, where $\xi^\star$ is one of the bounds of ξ. However, further investigation has shown that, although the ellipses defined by each $\mathbf{P}(\xi)$ have small major and minor axes (i.e., the cost associated with $\tilde{\mathbf{z}}(t)^T\mathbf{P}(\xi)\tilde{\mathbf{z}}(t)$ increases) with increasing $|\xi|$, they also intersect, due to a slight rotation around the origin that depends on ξ. This means that there is a subset where the maximum cost is not always in the extremes of the domain and the optimization is not convex anymore.

Our approach to find such $\bar{P}$ is to let $\bar{\mathbf{P}}=\beta\mathbf{P}(\xi')$, $\xi'\in\Xi$, where a $\beta>1$ is chosen such that (27) holds. To find the closed-form expression for $\mathbf{P}(\xi)$ for all $\xi\in\Xi$, the associated algebraic Riccati equation is solved symbolically and the only positive definite solution is chosen. Fig. 5 shows the largest eigenvalues of the left-hand side of the inequality (27), for all possible $\xi\in\Xi$ and $\xi'\in\Xi$ as a function of β, when input constraints are ignored. Also, the influence of $\mathbf{Q}$ and $\mathbf{R}$ on the eigenvalues of the left-hand side of (27) is investigated. It can be seen that the evolution of the maximum eigenvalue depending on β is monotonically decreasing. The inequality (27) is only satisfied when all the eigenvalues of the left-hand side are nonpositive. In fact, one of the eigenvalues is always negative. The other eigenvalue is negative for most β but can be positive for β values close to 1. The results are analogous when input rate constraints are considered, with one more negative eigenvalue.

Fig. 6 shows the eigenvalues of the left-hand side of inequality (25) for a fixed $\beta=1.2$ and ignoring input rate constraints. The eigenvalues of the left-hand side of the inequality (25) are computed as a function of ξ for each ξ'. The eigenvalues of the left-hand side matrix are always negative, which means that the inequality (25) is satisfied when using $\beta=1.2$. The results are analogous when input rate constraints are considered, with one more negative eigenvalue.

Note that it is possible to compute the smallest $\beta>1$ such that (27) holds. However, in practice, the vehicle prediction differs from the actual vehicle motion. Then, β should be chosen such that a conservative estimate of infinite-horizon cost (22) is achieved.

When input rate constraints are considered, the terminal cost term includes not only the terminal states, but also the terminal input. Therefore, the MPC cost function (11a) needs to be modified. Let $\mathbf{w}=\big[\tilde{\mathbf{z}}_{t+N|t}\ \tilde{\mathbf{u}}_{t+N-1|t}\big]^T$, then the terminal cost term becomes $\mathbf{w}^T\mathbf{Q}_f\mathbf{w}$.

5. Closed-loop stability and feasibility using an LTV-MPC scheme

In this section, Lyapunov techniques are used to prove closed-loop stability of the proposed LTV-MPC scheme (11), following the notation and argumentation flow used in Borrelli et al. (2017). The terminal constraint and terminal cost are determined via the methods explained in Section 4.

Assumption 1. The state penalization matrices $\mathbf{Q}$ and $\mathbf{Q}_f$ and the input penalization matrix $\mathbf{R}$ are symmetric positive definite, i.e., $\mathbf{Q}=\mathbf{Q}^T\succ 0$, $\mathbf{Q}_f=\mathbf{Q}_f^T\succ 0$, and $\mathbf{R}=\mathbf{R}^T\succ 0$.

Assumption 2. The sets $\tilde{\mathcal{Z}}$, $\tilde{\mathcal{Z}}_f$, and $\mathcal{U}$ are closed and contain the origin in their interior.

Assumption 3. $\tilde{\mathcal{Z}}_f$ is control invariant and $\tilde{\mathcal{Z}}_f\subset\tilde{\mathcal{Z}}$.

Assumption 4. There is no model mismatch between the prediction model and the plant model, i.e,

$$\begin{aligned}\mathbf{A}\big(\xi(k|t)\big)&=\mathbf{A}\big(\xi(k-n|t+n)\big),\\ \mathbf{B}\big(\xi(k|t)\big)&=\mathbf{B}\big(\xi(k-n|t+n)\big),\end{aligned} \tag{28}$$

for all $t>0$, $k=t,\dots,t+N-1$, and $n=0,\dots,k-1$.

To prove closed-loop stability of the MPC controller under the proposed terminal constraints and terminal cost, it is necessary to ensure recursive feasibility of the controller (i.e., the computed control

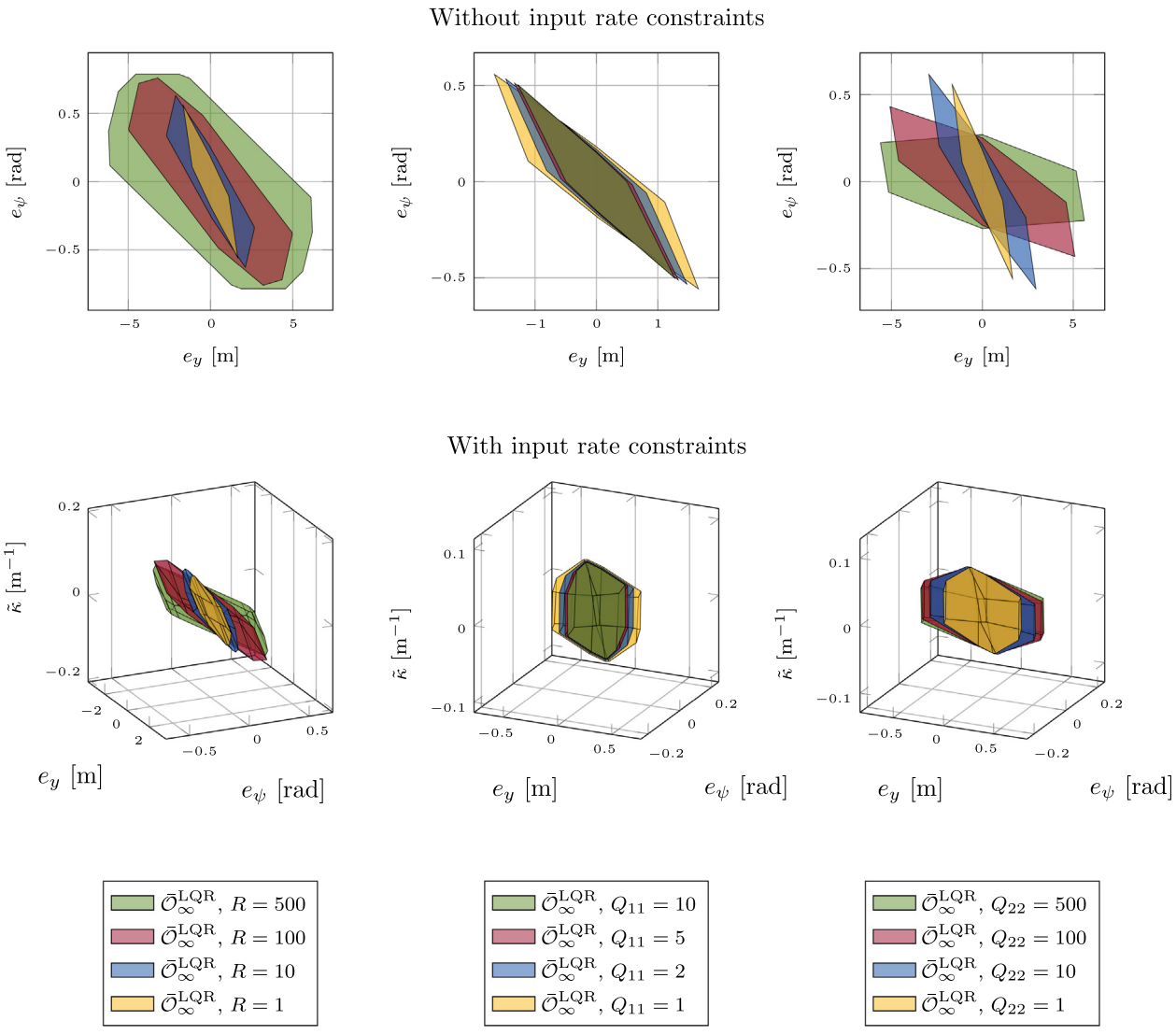

Fig. 3. Maximum positive invariant set for all $\gamma \in \Gamma$. On the top, LTV invariant set *ignoring* input rate constraints. Below, LTV invariant set *considering* input rate constraints. On the left, the input penalization matrix $\mathbf{R}$, which is related to the curvature κ, is varied. On the center, the first element of the state penalization matrix $\mathbf{Q}$, which is related to the lateral displacement e_y, is varied. On the right, the second element of the state penalization matrix $\mathbf{Q}$, which is related to the heading displacement e_ψ, is varied.

sequence $\tilde{U}_{t+1}^\star$ is feasible at time $t+1$ whenever the optimization at time t is feasible).

Theorem 5.1 (*LTV-MPC Feasibility*). *The problem (11) is feasible for all $t \geq 0$ if $\mathbf{Q}_f = \bar{\mathbf{P}}$, $\tilde{\mathcal{Z}}_f = \bar{\mathcal{O}}_\infty^{\mathrm{LQR}}$, and if $\mathbf{z}(0) \in \mathcal{K}_N(\bar{\mathcal{O}}_\infty^{\mathrm{LQR}})$.*

Proof. If $\mathbf{z}(0) \in \mathcal{K}_N(\bar{\mathcal{O}}_\infty^{\mathrm{LQR}})$, then the system is feasible at $t = 0$ (i.e., there exists a sequence of N inputs that brings the system to the set $\bar{\mathcal{O}}_\infty^{\mathrm{LQR}}$). By definition of $\bar{\mathcal{O}}_\infty^{\mathrm{LQR}}$, the system constraints are instantaneously satisfied at all points in $\bar{\mathcal{O}}_\infty^{\mathrm{LQR}}$, and $\bar{\mathcal{O}}_\infty^{\mathrm{LQR}}$ is invariant under the control law $\mathbf{u}(t) = \mathbf{l}_{\mathrm{LQR}}(\boldsymbol{\xi})\tilde{\mathbf{z}}(t), \forall \boldsymbol{\xi} \in \Xi$, since $\bar{\mathcal{O}}_\infty^{\mathrm{LQR}} \subset \mathcal{O}_\infty^{\mathrm{LQR}}$. Thus, the system is feasible for all $t \geq 0$. □

Theorem 5.2 (*Closed-loop Stability of the LTV-MPC Scheme*). *Consider the model (7), its constraints (2), and the LTV-MPC controller (11). Let Assumptions 1–4 hold. The terminal penalty matrix $\mathbf{Q}_f$ is chosen as $\bar{\mathbf{P}}$, and the terminal constraint $\tilde{\mathcal{Z}}_f$ is chosen as $\bar{\mathcal{O}}_\infty^{\mathrm{LQR}}$ Then, the state of the closed-loop system converges to the origin. Moreover, the origin of the closed-loop system is asymptotically stable with domain of attraction $\mathcal{K}_N(\bar{\mathcal{O}}_\infty^{\mathrm{LQR}})$.*

Proof. Consider problem (11) at time t. The argument $\boldsymbol{\xi}(t)$ from $\mathbf{A}$ and $\mathbf{B}$ is dropped for the sake of simplicity. Let $\mathbf{z}(t) \in \mathcal{K}_N(\bar{\mathcal{O}}_\infty^{\mathrm{LQR}})$ and let $\tilde{U}_t^\star = \{\tilde{\mathbf{u}}_{k|t}^\star\}_{k=t}^{t+N-1}$ be the optimizer of problem (11) and $\tilde{Z}_t^\star = \{\tilde{\mathbf{z}}_{k|t}^\star\}_{k=t}^{t+N}$ be the corresponding optimal state path. After the implementation of $\tilde{\mathbf{u}}(t) = \tilde{\mathbf{u}}_{t|t}^\star$ and using Assumption 4, $\tilde{\mathbf{z}}(t+1) = \tilde{\mathbf{z}}_{t+1|t} = \mathbf{A}\tilde{\mathbf{z}}(t) + \mathbf{B}\tilde{\mathbf{u}}_{t|t}^\star$ is obtained. Let $J_N^\star\big(\tilde{\mathbf{z}}(t)\big)$ be the optimal total predicted cost of (11a) when applying the $\tilde{U}_t^\star$ to the system state $\tilde{\mathbf{z}}(t)$.

Consider now problem (11) for $t+1$ and let us construct an upper bound on $J_N^\star\big(\tilde{\mathbf{z}}(t+1)\big)$. Consider the sequence

$$\tilde{U}_{t+1} = \{\tilde{\mathbf{u}}_{t+1|t}^\star, \dots, \tilde{\mathbf{u}}_{t+N|t}^\star, \mathbf{l}_{\mathrm{LQR}}\tilde{\mathbf{z}}_{t+N|t}^\star\}$$

and the corresponding state trajectory resulting from the initial state $\mathbf{z}(t+1)$,

$$\tilde{Z}_{t+1} = \{\tilde{\mathbf{z}}_{t+1|t}^\star, \dots, \tilde{\mathbf{z}}_{t+N|t}^\star, (\mathbf{A} + \mathbf{B}\mathbf{l}_{\mathrm{LQR}})\tilde{\mathbf{z}}_{t+N|t}^\star\},$$

where $\mathbf{l}_{\mathrm{LQR}}$ is the LQR feedback control law for the corresponding $\boldsymbol{\xi}$ at $t+N+1$. Let $J_N\big(\tilde{\mathbf{z}}(t+1)\big)$ be the predicted cost (11a) when applying $\tilde{U}_{t+1}$ to $\tilde{\mathbf{z}}(t+1)$. It is necessary to show that $J_N^\star\big(\tilde{\mathbf{z}}(t)\big)$ is a Lyapunov function for the closed-loop system. With direct calculations it is possible to derive

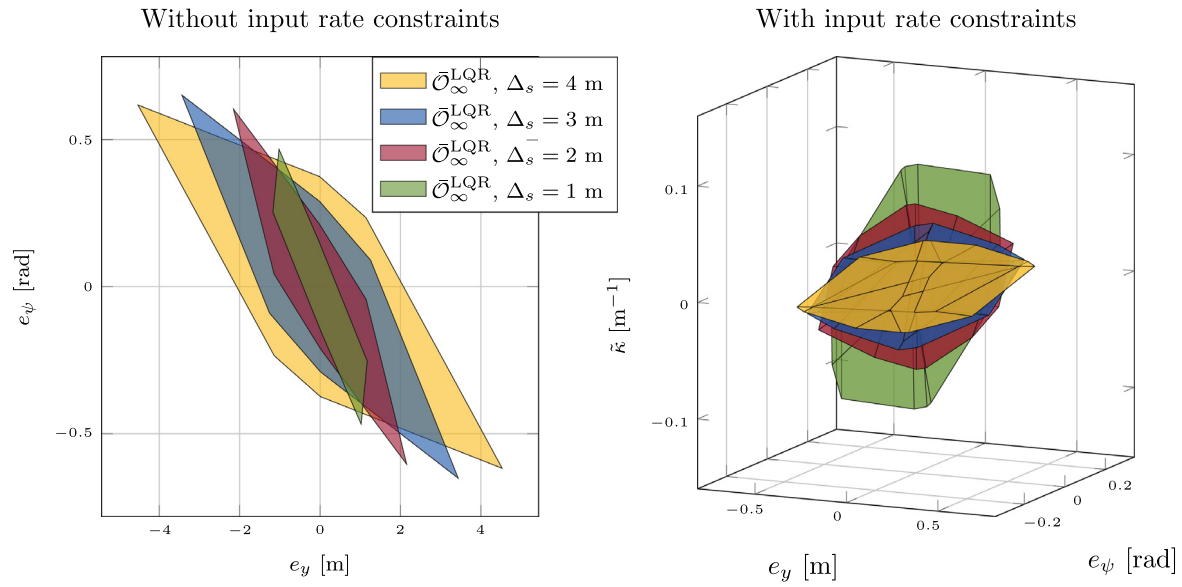

Fig. 4. Maximum positive invariant set for all $\gamma \in \Gamma$ for different sampling distances $\Delta_s = vT_s$. On the left, LTV invariant set not considering input rate constraints. On the right, LTV invariant set considering input rate constraints.

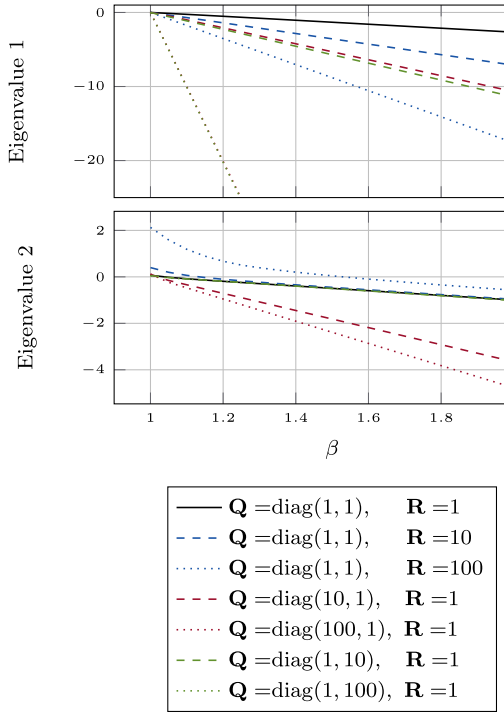

Fig. 5. Largest eigenvalues of the left-hand side of the inequality (27). When both eigenvalues are nonpositive the inequality (25) is satisfied.

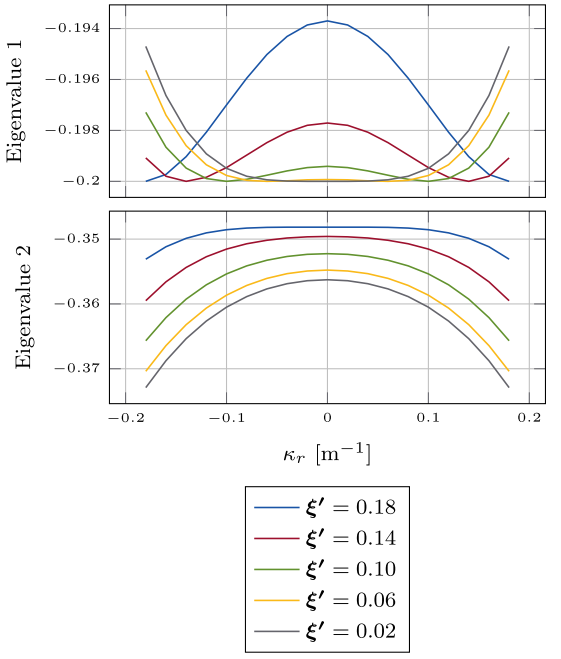

Fig. 6. Eigenvalues of the left-hand side of the inequality (25) for different $\xi' = \kappa_r$ as a function of $\xi = \kappa_r$ and $\beta = 1.2$. The eigenvalues are always negative, so the inequality (25) is satisfied.

the following result

$$\begin{aligned} J_N\big(\tilde{\mathbf{z}}(t+1)\big) =& J_N^\star\big(\tilde{\mathbf{z}}(t)\big) - (\tilde{\mathbf{z}}_{t|t}^T \mathbf{Q}\tilde{\mathbf{z}}_{t|t} + \tilde{\mathbf{u}}_{t|t}^{*T} \mathbf{R}\tilde{\mathbf{u}}_{t|t}^\star) \\ &+ \tilde{\mathbf{z}}_{t+N|t}^T \big((\mathbf{A}+\mathbf{B}\mathbf{l}_{\mathrm{LQR}})^T \bar{\mathbf{P}}(\mathbf{A}+\mathbf{B}\mathbf{l}_{\mathrm{LQR}}) + \mathbf{Q} \\ &+ \mathbf{l}_{\mathrm{LQR}}^T \mathbf{R}\mathbf{l}_{\mathrm{LQR}} - \bar{\mathbf{P}}\big)\tilde{\mathbf{z}}_{t+N|t}, \end{aligned} \tag{29}$$

where, if $\beta > 1$ is chosen as explained in Section 4.3,

$$\begin{aligned} \tilde{\mathbf{z}}_{t+N|t}^T \bar{\mathbf{P}} \tilde{\mathbf{z}}_{t+N|t} \geq \tilde{\mathbf{z}}_{t+N|t}^T \big((\mathbf{A}+\mathbf{B}\mathbf{l}_{\mathrm{LQR}})^T \bar{\mathbf{P}}(\mathbf{A}+\mathbf{B}\mathbf{l}_{\mathrm{LQR}}) + \mathbf{Q} \\ + \mathbf{l}_{\mathrm{LQR}}^T \mathbf{R}\mathbf{l}_{\mathrm{LQR}}\big)\tilde{\mathbf{z}}_{t+N|t} > 0, \end{aligned} \tag{30}$$

and therefore, since $\bar{\mathbf{P}}$ gives the largest infinite-horizon predicted cost with respect to all systems $\gamma \in \Gamma$,

$$J_N\big(\tilde{\mathbf{z}}(t+1)\big) \leq J_N^\star\big(\tilde{\mathbf{z}}(t)\big) - (\tilde{\mathbf{z}}_{t|t}^T \mathbf{Q}\tilde{\mathbf{z}}_{t|t} + \tilde{\mathbf{u}}_{t|t}^{*T} \mathbf{R}\tilde{\mathbf{u}}_{t|t}^\star), \tag{31}$$

and since, by construction, $J_N^\star\big(\tilde{\mathbf{z}}(t+1)\big) \leq J_N\big(\tilde{\mathbf{z}}(t+1)\big)$,

$$J_N^\star\big(\tilde{\mathbf{z}}(t+1)\big) - J_N^\star\big(\tilde{\mathbf{z}}(t)\big) \leq -(\tilde{\mathbf{z}}_{t|t}^T \mathbf{Q}\tilde{\mathbf{z}}_{t|t} + \tilde{\mathbf{u}}_{t|t}^{*T} \mathbf{R}\tilde{\mathbf{u}}_{t|t}^\star), \tag{32}$$

where the right-hand side is clearly negative definite due to the positive definiteness of $\mathbf{Q}$ and $\mathbf{R}$.

Assumption 1 and (32) ensure that $J_N^\star\big(\tilde{\mathbf{z}}(t)\big)$ strictly decreases along the state trajectories of the closed-loop system (16) for any $\tilde{\mathbf{z}} \in \mathcal{K}_N(\bar{\mathcal{O}}_\infty^{\mathrm{LQR}})$, $\tilde{\mathbf{z}} \neq 0$. In addition to the fact that $J_N^\star\big(\tilde{\mathbf{z}}(t)\big)$ decreases, it

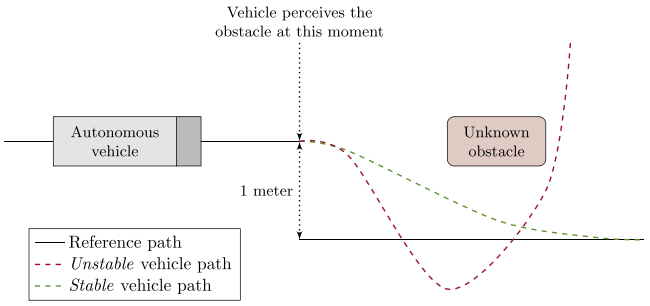

Fig. 7. Emergency obstacle avoidance scenario illustration. The vehicle travels at constant speed in a straight line. Suddenly, an obstacle appears in front of the vehicle.

is also lower-bounded by zero and the state trajectories generated by the closed-loop system (16) starting from any $\tilde{\mathbf{z}}(0) \in \mathcal{K}_N(\bar{\mathcal{O}}_\infty^{\mathrm{LQR}})$ lie in $\mathcal{K}_N(\bar{\mathcal{O}}_\infty^{\mathrm{LQR}})$ for all $t \geq 0$. Assumptions 2 and 3 and Eq. (32) are sufficient to ensure that the state of the closed-loop system converges to the origin as $t \to \infty$ if the initial state lies in $\mathcal{K}_N(\bar{\mathcal{O}}_\infty^{\mathrm{LQR}})$.

Lyapunov theory is used to show that the origin of the closed-loop system (16) is asymptotically stable. $J_N^\star(\tilde{\mathbf{z}}(t))$ is positive definite due to Assumption 1. Furthermore, (32) states that $J_N^\star(\tilde{\mathbf{z}}(t))$ decreases along the closed-loop trajectories. Then, $\tilde{\mathbf{z}}_{t|t}^T \mathbf{Q} \tilde{\mathbf{z}}_{t|t} + \tilde{\mathbf{u}}_{t|t}^{\star T} \mathbf{R} \tilde{\mathbf{u}}_{t|t}^\star \to 0$ as $t \to \infty$. □

6. LTV-MPC design evaluation

This section demonstrates the effectiveness of using the terminal constraint $\tilde{\mathcal{Z}}_f = \bar{\mathcal{O}}_\infty^{\mathrm{LQR}}$ and cost $\mathbf{Q}_f = \bar{\mathbf{P}}$ both in simulation and experimentally. The evaluation is done in a scenario that resembles an emergency scenario (see Fig. 7). The vehicle travels in a straight line and suddenly a fictitious obstacle appears in front, forcing the vehicle to steer away from it. For purposes of experiment repeatability, the vehicle, at the moment of obstacle perception, always steers from a straight line to another straight line located one meter apart. The MPC does not have any preview information about when this change is supposed to happen. The driving performance (e.g., accuracy or smoothness) is not the focus of our analysis, but yet clear evidence of (in)stability is sought. Both in simulation and experimentally, the vehicle drives with a constant speed of 8 m/s. The road-aligned kinematic model (14) is used as a prediction model. The only parameter modified in each run is the first element of the state penalization matrix Q_{11}, which accounts for the penalization of the vehicle lateral displacement e_y with respect to the reference path. The other parameters are $Q_{22} = 10$ and $\mathbf{R} = 10$, and the prediction horizon is $N = 3$ steps, using a spatial discretization of $\Delta_s = 1.6$ m. In this scenario, only Q_{11} is changed, since larger Q_{22} or R yield less aggressive control and consequently stable behavior.

The terminal state constraints and cost are computed offline, the controller runs at 50 Hz, and each MPC optimization is solved using qpOASES (Ferreau, Kirches, Potschka, Bock, & Diehl, 2014). For practical reasons (i.e., to ensure feasibility all the time), a slack variable is included in the terminal constraints (11e) and penalized quadratically in the cost function (11a). The initial tuning is such that the MPC without terminal constraint and cost is stable. A comparison is made between the MPC controllers (11) with and without terminal constraint and cost.

Remark. In this scenario, the prediction model is LTI, since the reference path is a straight line. However, from the point of view of the MPC, the reference path is unknown after the last point of the prediction horizon and can have any (bounded) curvature. So, stability is guaranteed according to Theorem 5.2.

For the sake of simplicity, in the remainder of the section, the controllers are referred as follows:

Fig. 8. Modified Scania G480 construction truck used as experimental and research platform.

- *Controller A* — LTV-MPC *without* terminal cost and terminal state set;
- *Controller B* — LTV-MPC *with* terminal cost and terminal state set *ignoring* input rate constraints;
- *Controller C* — LTV-MPC *with* terminal cost and terminal state set *considering* input rate constraints.

6.1. Simulation results

A fundamental step before deploying the controller on a real vehicle is simulation evaluation. The same MATLAB/Simulink simulation environment thoroughly presented in Lima and Trincavelli et al. (2017) is used. There, the system architecture is described and the simulation environment is shown to be sufficiently accurate to allow the controller evaluation and tuning before deploying it on the vehicle. The vehicle is simulated using a 4-axles nonlinear bicycle model with 2 steering axles in the front and 2 traction axles in the back, which is based on a modified Scania G480 construction truck (Lima, Trincavelli, Mårtensson, & Wahlberg, 2015) that can be seen in Fig. 8.

Fig. 9 shows the deviation from the path and the steering angle computed during the simulation. It is clear that the performance differences between using or not terminal cost and terminal state set when $Q_{11} = 1$ are marginal. However, at $Q_{11} = 5$ the differences in performance are more noticeable, where controllers B and C converge to the reference path, while controller A is unstable. In fact, note that controller C overshoots much less than controller B, due to the knowledge of the input rate constraints. Increasing Q_{11}, controller A is still unstable and controller B overshoots even more, while controller C keeps the same performance as before. Due to the knowledge of the input rate constraints, controller C is much less aggressive than controllers A or B (i.e., much longer rise time), which ultimately yields stability.

Note that, simulating a nonlinear model with dynamics, the Assumption 4 of no model mismatch does not hold anymore. Even though, the control design yields closed-loop stability, since it is a conservative approach, as it considers all possible models to construct the terminal state set and cost. This resembles, in some aspects, the tube-based robust MPC schemes (Mayne, Seron, & Raković, 2005). In the robust MPC scheme, the state and input constraints set is *shrunk* depending on the upper-bound of disturbance subject to the system. In the LTV-MPC case, the terminal state set is also smaller and contained inside the terminal constraint set of each LTI model individually. In summary, there is some inherent robustness in this approach. Its quantification lies outside of the scope of this work, but will be considered as a subject of future research.

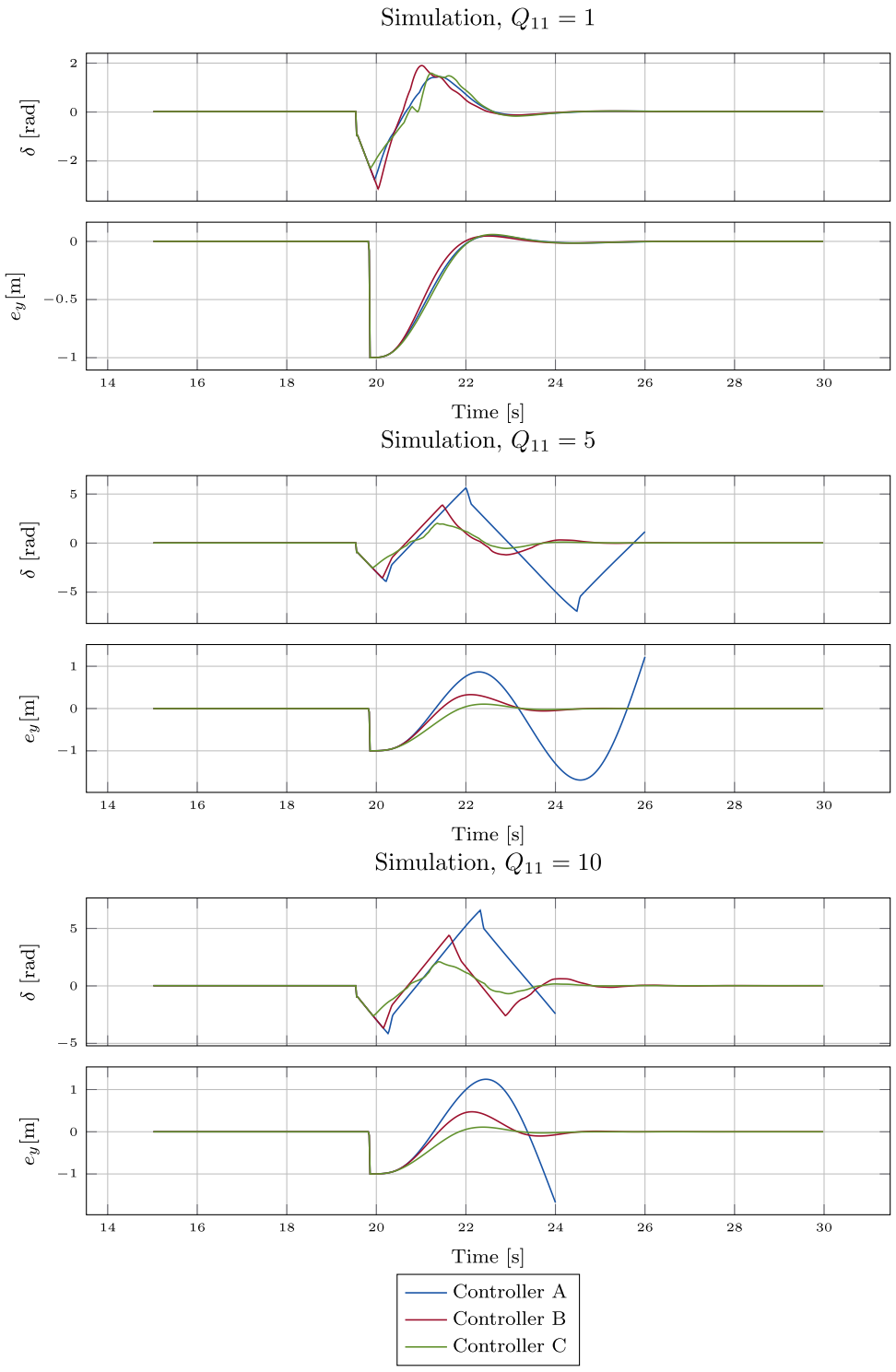

Fig. 9. *Simulation* of the MPC controller (11). Just before 20 s of simulation, the obstacle is detected and one meter reference change happens. The effectiveness of the terminal cost and terminal state set (with and without input rate constraints) derived in Sections 4.2 and 4.3 are evaluated for different MPC parameter tuning.

6.2. Experimental results

The truck used in the experimental evaluation is a modified Scania G480 construction truck and is shown in Fig. 8. The vehicle is equipped with a sensor platform and a servo motor for automated control of the steering column. The reference path, consisted of two straight lines one meter apart, is generated offline and is located at Scania's test facilities in Södertälje, Sweden. Fig. 10 shows the deviation from the path and the steering angle computed during the experiment. The main conclusions from the simulation analysis are, in general, also valid here. The main difference is that, when increasing Q_{11}, controller B becomes unstable earlier. It is clear that controller C is stable for the different parameter tunings evaluated. A video of the experiment is available on Zenodo (Lima, Collares Pereira, Mårtensson, and Wahlberg, 2017).

Note that the prediction horizon used, $N\Delta_s = 4.8$ m, is a fairly short one. In this particular scenario, increasing the prediction horizon in general yields a stable system. In fact, Lima and Trincavelli et al. (2017) shows experiments where an autonomous truck with an MPC

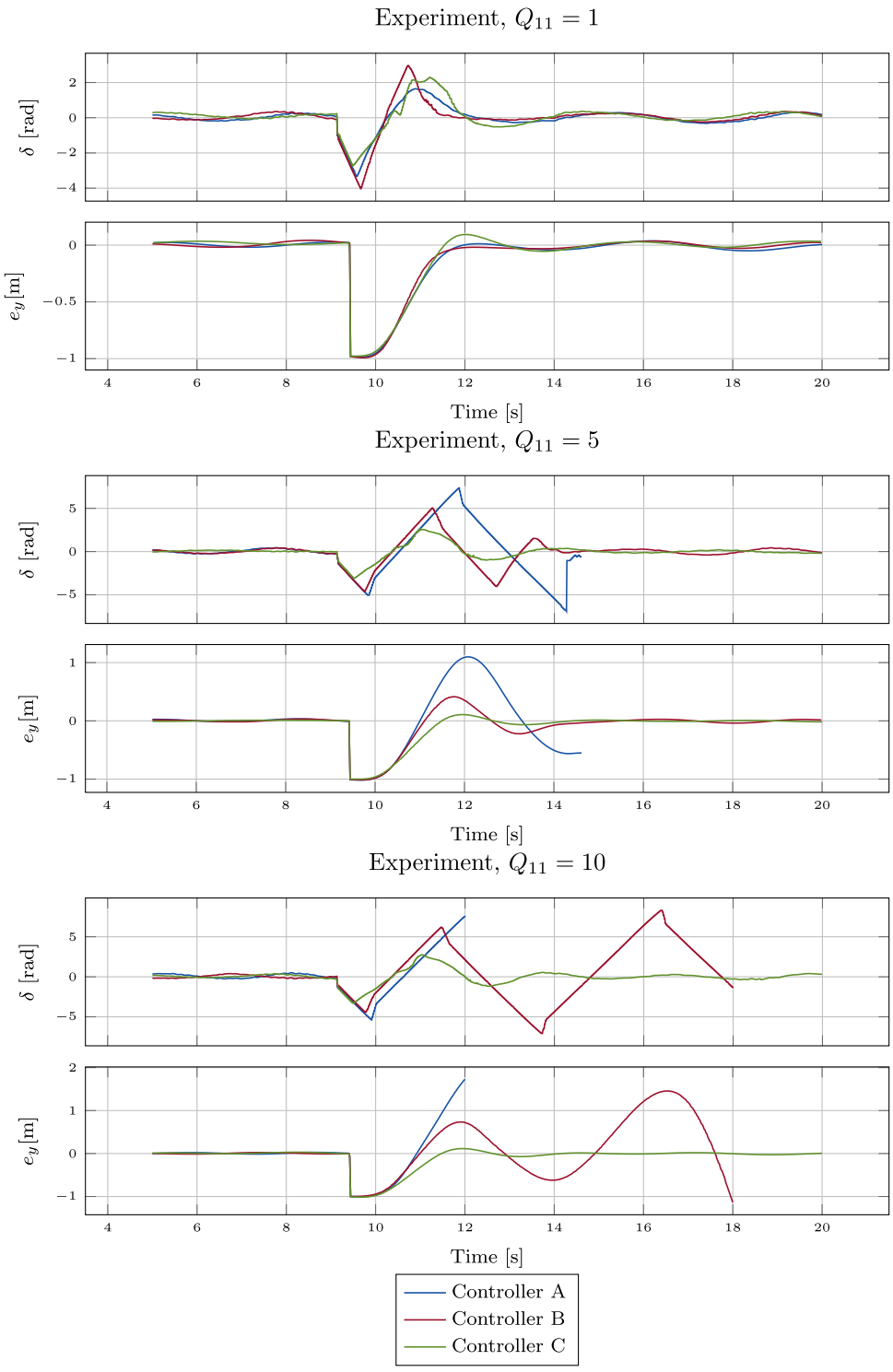

Fig. 10. *Experiment* of the MPC controller (11). Just before 10 s of simulation, the obstacle is detected and one meter reference change happens. The effectiveness of the terminal cost and terminal state set (with and without input rate constraints) derived in Sections 4.2 and 4.3 are evaluated for different MPC parameter tuning.

is stable without terminal cost and terminal state set and $N = 10$. To possibly induce instability using larger prediction horizon steps, it would be required to drive faster and perform more aggressive and dangerous maneuvers. However, it is not desirable to perform such experiments due to safety reasons. In practice, the same reasoning about robustness provided in the simulation results section holds.

7. Conclusions and future work

This paper investigated the design of the terminal cost and terminal state set when designing and implementing a reference tracking LTV-MPC for an autonomous vehicle such that closed-loop stability is guaranteed. To predict the vehicle motion in the MPC, a linearized version of a nonlinear space-based kinematic model on a road-aligned

coordinate frame was used. The determination of the terminal constraint and cost is performed using a multi-model representation that spans the possible LTI vehicle models within a predefined parameter range. The terminal constraint is the maximal positive invariant set for all the models in the multi-model description. The terminal cost is the upper-bound on the cost-to-go incurred by applying an LQR control law to any of the possible models in the multi-model representation. The upper-bound was obtained by positively scaling one of Riccati matrices resulting from cost-to-go calculation. By including the terminal cost and terminal state set in the controller formulation, closed-loop asymptotic stability of the LTV-MPC scheme is proved through Lyapunov arguments. Finally, the proposed control design was evaluated in simulation and experimentally. The scenario considered resembled an emergency situation, where at constant speed, the vehicle had to avoid a fictitious obstacle. The effectiveness of the terminal cost and terminal state set that include the input rate constraints was clear. When the terminal cost and terminal state set were not used, increasing controller aggressiveness led to controller instability, even when using terminal cost and terminal state set without considering input rate constraints. On the other hand, when using the terminal cost and terminal state set that consider the input rate constraints, the controller was always stable.

As future work, it would be interesting to investigate these conditions in the light of robust MPC to explicitly include the influence of model uncertainties in the controller performance, since the prediction model is simplistic. For the same reason, it would be relevant to analytically compute bounds for the parameter β depending on the model robustness in practice. Furthermore, current research is looking into proving closed-loop stability when the sampling distance Δs and, consequently, the vehicle speed, is also a parameter.

Acknowledgments

We would like to thank Soheil Salehpour, a development engineer at Scania CV AB, for the invaluable help during the experimental evaluation of the controller. We would also like to thank Yuchao Li, a Ph.D. student in the Automatic Control department at KTH, for the interesting discussions and for double checking the theoretical proofs.

References

Ai, B., Sentis, L., Paine, N., Han, S., Mok, A., & Fok, C. -L. (2016). Stability and performance analysis of time-delayed actuator control systems. *Journal of Dynamic Systems, Measurement, and Control*, *138*(5).

Badgwell, T. A., & Thomas, A. (1997). Robust model predictive control of stable linear systems. *International Journal of Control*, *68*(4), 797–818.

Beal, C., & Gerdes, J. (2013). Model predictive control for vehicle stabilization at the limits of handling. *IEEE Transactions on Control Systems Technology*, *21*(4), 1258–1269.

Bemporad, A. (2006). Model predictive control design: New trends and tools. In *Proceedings of the IEEE annual conference on decision and control* (pp. 6678–6683).

Blanchini, F. (1999). Survey paper: Set invariance in control. *Automatica*, *35*(11), 1747–1767.

Borrelli, F., Bemporad, A., & Morari, M. (2017). *Predictive control for linear and hybrid systems*. Cambridge University Press.

De Luca, A., Oriolo, G., & Samson, C. (1998). *Feedback control of a nonholonomic car-like robot, Vol. 229* (pp. 171–253). Springer Berlin Heidelberg, (Ch. 4).

European Commission, (2011). Roadmap to a Single European Transport Area, http://ec.europa.eu/transport/strategies/facts-and-figures/index_en.htm.

Falcone, P., Borrelli, F., Asgari, J., Tseng, H. E., & Hrovat, D. (2007). Predictive active steering control for autonomous vehicle systems. *IEEE Transactions on Control Systems Technology*, *15*(3), 566–580.

Falcone, P., Borrelli, F., Tseng, E., Asgari, J., & Hrovat, D. (2008a). A hierarchical model predictive control framework for autonomous ground vehicles. In *Proceedings of the American control conference* (pp. 3719–3724).

Falcone, P., Borrelli, F., Tseng, H., Asgari, J., & Hrovat, D. (2008b). Linear time-varying model predictive control and its application to active steering systems: Stability analysis and experimental validation. *International Journal of Robust and Nonlinear Control*, *18*(8), 862–875.

Ferreau, H., Kirches, C., Potschka, A., Bock, H., & Diehl, M. (2014). qpOASES: A parametric active-set algorithm for quadratic programming. *Mathematical Programming Computation*, *6*(4), 327–363.

Frasch, J. V., Gray, A., Zanon, M., Ferreau, H. J., Sager, S., Borrelli, F., et al. (2013). An auto-generated nonlinear MPC algorithm for real-time obstacle avoidance of ground vehicles. In *IEEE European control conference* (pp. 4136–4141).

Funke, J., Brown, M., Erlien, S. M., & Gerdes, J. C. (2017). Collision avoidance and stabilization for autonomous vehicles in emergency scenarios. *IEEE Transactions on Control Systems Technology*, *25*(4), 1204–1216.

Gao, Y., Gray, A., Frasch, J., Lin, T., Tseng, E., Hedrick, J., et al. (2012). Spatial predictive control for agile semi-autonomous ground vehicles. In *Proceedings of the international symposium on advanced vehicle control*.

Garcia, C., Prett, D., & Morari, M. (1989). Model predictive control: theory and practice - a survey. *Automatica*, *25*(3), 335–348.

Katriniok, A., Maschuw, J. P., Christen, F., Eckstein, L., & Abel, D. (2013). Optimal vehicle dynamics control for combined longitudinal and lateral autonomous vehicle guidance. In *Proceedings of the European control conference* (pp. 974–979). IEEE.

Keerthi, S. S., & Gilbert, E. G. (1988). Optimal infinite-horizon feedback laws for a general class of constrained discrete-time systems: Stability and moving-horizon approximations. *Journal of Optimization Theory and Applications*, *57*(2), 265–293.

Kolmanovsky, I., & Gilbert, E. G. (1998). Theory and computation of disturbance invariant sets for discrete-time linear systems. *Mathematical Problems in Engineering*, *4*(4), 317–367.

Kothare, M. V., Balakrishnan, V., & Morari, M. (1996). Robust constrained model predictive control using linear matrix inequalities. *Automatica*, *32*(10), 1361–1379.

Kvasnica, M., Grieder, P., Baotić, M., & Morari, M. (2004). Multi-parametric toolbox (MPT). In *International workshop on hybrid systems: Computation and control* (pp. 448–462). Springer.

Lima, P. F., Collares Pereira, G., Mårtensson, J., & Wahlberg, B. (Oct. 2017). Experimental Evaluation LTV-MPC Stability for Autonomous Driving. http://dx.doi.org/10.5281/zenodo.1292428, URL https://zenodo.org/record/1292428.

Lima, P. F., Mårtensson, J., & Wahlberg, B. (2017). Stability conditions for linear time-varying model predictive control in autonomous driving. In *Proceedings of the IEEE conference on decision and control*.

Lima, P. F., Oliveira, R., Mårtensson, J., Bemporad, A., & Wahlberg, B. (2017). Minimizing long vehicles overhang exceeding the drivable surface via convex path optimization. In *Proceedings of the international IEEE intelligent transportation systems conference*.

Lima, P. F., Trincavelli, M., Mårtensson, J., Nilsson, M., & Wahlberg, B. (2017). Spatial model predictive control for smooth and accurate steering of and autonomous truck. *IEEE Transactions on International Vehicles*, *2*(4), 238–250.

Lima, P. F., Trincavelli, M., Mårtensson, J., & Wahlberg, B. (2015). Clothoid-based model predictive control for autonomous driving. In *Proceedings of the European control conference* (pp. 2983–2990).

Liniger, A., Domahidi, A., & Morari, M. (2015). Optimization-based autonomous racing of 1:43 scale RC cars. *Optimal Control Applications and Methods*, *36*(5), 628–647.

Lu, Y., & Arkun, Y. (2000). Quasi-min-max MPC algorithms for LPV systems. *Automatica*, *36*(4), 527–540.

Mayne, D., Rawlings, J., Rao, C., & Scokaert, P. (2000). Constrained model predictive control: Stability and optimality. *Automatica*, *36*(6), 789–814.

Mayne, D. Q., Seron, M. M., & Raković, S. V. (2005). Robust model predictive control of constrained linear systems with bounded disturbances. *Automatica*, *41*(2), 219–224.

Mchugh, M. (2015). Tesla's cars now drive themselves, kinda, Wired, http://www.wired.com/2015/10/tesla-self-driving-over-air-update-live/.

Plessen, M. G., Lima, P. F., Mårtensson, J., Bemporad, A., & Wahlberg, B. (2017). Trajectory planning under vehicle dimension constraints using sequential linear programming. In *Proceedings of the international IEEE intelligent transportation systems conference*.

Pluymers, B., Rossiter, J. A., Suykens, J. A. K., & De Moor, B. (2005). The efficient computation of polyhedral invariant sets for linear systems with polytopic uncertainty. In *Proceedings of the IEEE American control conference* (pp. 804–809).

Ross, P. (2014). Robot, you can drive my car. *IEEE Spectrum*, *51*(6), 60–90.

Thrun, S., Montemerlo, M., Dahlkamp, H., Stavens, D., Aron, A., Diebel, J., et al. (2006). Stanley: The robot that won the DARPA grand challenge. *Journal of Field Robotics*, *23*(9), 661–692. http://dx.doi.org/10.1002/rob.v23:9.

Turri, V., Carvalho, A., Tseng, E., Johansson, K., & Borrelli, F. (2013). Linear model predictive control for lane keeping and obstacle avoidance on low curvature roads. In *Proceedings of the international IEEE intelligent transportation systems conference* (pp. 378–383).

Urmson, C., Bagnell, J., Baker, C., Hebert, M., Kelly, A., Rajkumar, R., et al. (2007). Tartan racing: A multi-modal approach to the DARPA urban challenge, Tech. rep., Carnegie Mellon University.

Verschueren, R., De Bruyne, S., Zanon, M., Frasch, J. V., & Diehl, M. (2014). Towards time-optimal race car driving using nonlinear MPC in real-time. In *Proceedings of the conference on decision and control* (pp. 2505–2510).

World Health Organization, (2009). Global status report on road safety: Time for action, www.who.int/violence_injury_prevention/road_safety_status/2009.

Ziegler, C. (0000). Volvo will run a public test of self-driving cars with 100 real people in 2017, The Verge, http://www.theverge.com/2015/2/23/8091455/volvo-drive-me-self-driving-car-test-2017.

Ziegler, J., Bender, P., Schreiber, M., Lategahn, H., Strauss, T., Stiller, C., et al. (2014). Making Bertha drive 2014 - An autonomous journey on a historic route. *IEEE Intelligent Transportation Systems Magazine*, *6*(2), 8–20. http://dx.doi.org/10.1109/MITS.2014.2306552.